Synthesis of Isoreticular Metal Organic Framework-3 (IRMOF-3) Porous Nanostructure and Its Effect on Naphthalene Adsorption: Optimized by Response Surface Methodology

Masoomeh Yari Kalashgrani [1], Aziz Babapoor [1,*], Seyyed Mojtaba Mousavi [2], Solmaz Feizpoor [3], Seyyed Alireza Hashemi [4], Mojtaba Binazadeh [5], Wei-Hung Chiang [2] and Chin Wei Lai [6,*]

[1] Department of Chemical Engineering, University of Mohaghegh Ardabili, Ardabil 56199-11367, Iran; masoomeh.yari.72@gmail.com
[2] Department of Chemical Engineering, National Taiwan University of Science and Technology, Taipei 10607, Taiwan; kempo.smm@gmail.com (S.M.M.); whchiang@mail.ntust.edu.tw (W.-H.C.)
[3] Department of Chemistry, Faculty of Science, University of Mohaghegh Ardabili, Ardabil 56199-11367, Iran; feizpoorsolmaz@yahoo.com
[4] Nanomaterials and Polymer Nanocomposites Laboratory, School of Engineering, University of British Columbia, Kelowna, BC V1V 1V7, Canada; s.a.hashemi0@gmail.com
[5] Department of Chemical Engineering, School of Chemical and Petroleum Engineering, Shiraz University, Shiraz 71557-13876, Iran; binazadeh@shirazu.ac.ir
[6] Nanotechnology & Catalysis Research Centre, University of Malaya, Kuala Lumpur 50603, Malaysia
* Correspondence: babapoor@uma.ac.ir (A.B.); cwlai@um.edu.my (C.W.L.)

Abstract: Naphthalene is a carcinogenic compound and its environmental release poses a major risk to human and aquatic health. Therefore, the application of nanomaterial technologies for naphthalene removal from wastewater has attracted significant attention. In this research, for the first time, the performance of IRMOF-3 for naphthalene removal from aqueous media is evaluated. IRMOF-3 with a specific surface area of 718.11 $m^2 \cdot g^{-1}$ has the ability to absorb naphthalene from synthetic wastewater to a high extent. The structures and morphology of IRMOF-3 were determined by FT-IR, XRD, SEM and BET analyses. Thirty adsorption experiments were conducted to obtain the best conditions for naphthalene removal. An optimum naphthalene removal efficiency of 80.96% was obtained at IRMOF-3 amounts of 0.1 $g \cdot L^{-1}$, a solution concentration of 15 $mg \cdot L^{-1}$, a contact time of 60 min and a pH = 11. The results indicate that the lower the concentration of naphthalene, the higher its dispersion at the surface of the porous nanostructure. Increasing naphthalene concentration results in its accumulation on porous nanostructures that clog cavities. In addition, high contact time provides ample opportunity for naphthalene to penetrate the cavities and pores which facilitates crystallization phenomena deep in the pores. Finally, the results of this study revealed that IRMOF-3 is one of the most effective adsorbents for naphthalene removal from wastewater.

Keywords: environment; porous nanostructure; IRMOF-3; naphthalene; central composite design; adsorption

1. Introduction

Water contamination is a global challenge that endangers life [1–5]. Thus, rehabilitation of pollutants from soil and groundwater is very important for researchers and environmental agencies. Phenols, aliphatic polycyclic aromatic hydrocarbons (PAHs), heavy metal ions, and dyes in industrial wastewater seriously influence the quality of freshwater which ultimately threatens human beings, animals, and plant life [1,6–8]. Aromatic polycyclic hydrocarbons (PAHs) are carcinogenic chemical compounds with two to seven benzene rings [9,10]. Naphthalene is one of the aromatic hydrocarbons that is reportedly accumulated in estuaries and sediments environments. Upon groundwater contamination with petroleum compounds, naphthalene may enter drinking water sources and accumulate in adipose tissue through the food chain [11–13]. Although the concentration of this compound in water is very low,

its adverse impact is immense [14,15]. The standard for aromatic hydrocarbon compounds, including naphthalene, concentration in water is ≤0.1 mg/L [16–18]. Serious health problems such as hemolytic anemia in children and anemia are side effects of higher doses of naphthalene in water [19,20]. Therefore, it is crucial to develop (1) novel technologies that prevent naphthalene release into the environment and (2) effective methods for naphthalene removal from surface waters [21–23]. Proposed methods for removing naphthalene from wastewater include advanced oxidation processes, membrane separation, biological degradation and adsorption [24–28]. Adsorption processes using solid adsorbents compared to the other techniques have the merits of easy control, low operational cost, high elimination efficiency, and adsorbent recovery [29–31]. Therefore, adsorption is one of the most widely employed processes for organic contaminants removal from wastewater. Adsorbents like clay minerals, agricultural wastes, zeolites [32–35], activated carbon, graphene oxide (GO) and metal-organic frameworks (MOFs), have been reported for naphthalene removal from aqueous media [36–39]. By studying the aforesaid adsorbents, researchers are trying to synthesize and build a new group of adsorbents to achieve enhanced efficiencies in single and multiple solvent systems [40]. MOFs are one of the proposed new adsorbents that offer huge surface area, adjustable pore size, and tunable internal surface characteristics [41,42]. MOFs may be utilized in other applications including heterogeneous decomposition, separation, measurement, and molecular detection [43–45]. MOFs include a central metal atom and the organic molecule which is known as the ligand. The isoreticular metal organic framework-3 (IRMOF-3) is a popular MOF that exhibits good capability as an efficient adsorbent for wastewater treatment processes. IRMOF-3 adsorption ability is attributed to (1) the presence of 2-amino-benzenedicarboxylate linkers in its structure, (2) its 3D (three-dimensional) cubic porous framework consisting of secondary Zn_4O structural units [46,47], (3) unusual pore volume and large specific surface area, and (4) suitable thermal and mechanical stability [48,49].

Nowadays, statistical and engineering methods such as the surface response methodology (RSM) are used for process optimization. Using this method, a smaller number of tests are required and the interactions between different factors are considered [50–52]. In this way, the optimal values of each variable and its degree of importance can be easily determined [53,54]. In this study, the central composite design (CCD) and response-level method were employed. In the central composite design procedure, the principal goal is the evaluation of dependent responses and parameters optimization. In addition, in CCD design each factor is examined in five levels ($-\alpha$, -1, 0, $+1$, $+\alpha$) or, in the case of the facet center, in three levels (for $\alpha = 1$) where -1 and $+1$ are the upper and lower levels and $-\alpha$ and $+\alpha$ are the new limits of the factors. Point zero is considered the central point of the design.

Arizavi et al. [55] studied naphthalene adsorption from aqueous media with a kaolin/Fe_3O_4 composite using the central composite design. Their results indicated that increasing pH, exposure time or composite dose increases naphthalene adsorption. They reported the optimal conditions as 4.8 g·L^{-1} of composite dose, 66 min contact time, and pH 6.5

For a solution containing 10 mg·L^{-1} of naphthalene at the optimum condition, 97% elimination efficiency was obtained. Farzadkia et al. [56] reported optimum TPH removal efficiency of 49.90 ± 12.47% by modeling the ozonation process using RSM. Borousan et al. [57] modeled malachite green dye degradation using RSM. They reported that at optimum conditions IRMOF-3, IRMOF-3-MWCNT-OH and IRMOF-3-MWCNT-OH-Pd-NPs reveal adsorption efficiencies of 37.20%, 55.50% and 96.10%, respectively. Clearly, the degradation efficiency percentage enhances considerably upon adsorbent surface modification with MWCNT-OH and Pd nanoparticles. They also reported that IRMOF-3 does not offer any reusable potential, while IRMOF-3-MWCNT-OH and IRMOF-3-MWCNT-OH-Pd-NP possess three and five successive retrievals, respectively.

Ghaedi et al. [37] studied the applicability of zinc sulfide nanoparticles loaded activated carbon (ZnS-NPs-AC) for naphthalene removal from aqueous solution using RSM. In the quadratic CCD model, four independent parameters, namely pH (1.0–9.0), initial concentration of naphthalene (5–45 mg·L^{-1}), adsorbent dosage (0.005–0.025 g) and contact time (5–25 min) were coded to predict the response. Based on the results under the opti-

mum conditions of 0.02 g of adsorbent dose, 15 min contact time, pH 5.0 and 15 mg·L^{-1} of naphthalene, its adsorption on ZnS-NPs-AC results in 98.8% removal.

Rani et al. [58] studied naphthalene removal from aqueous solutions by using a slurry photocatalytic membrane reactor (coupling TiO$_2$/UV-C photocatalysis and ultrafiltration (UF) membrane process) that was studied by examining the effect of various parameters, intermediate identification and using the RSM approach. Various operating parameters such as initial NAP concentration (5–25 mg·L^{-1}), catalyst dosage (0.1–0.9 g·L^{-1}), and feed solution pH (3–9) were investigated for NAP removal. Experimental results obtained from the batch study of the integrated process showed 92.8% of NAP removal compared to individual processes. UV-TiO$_2$ (76.8% NAP removal) and UF membrane separation process (49.1% NAP removal) showed low removal rates for similar experimental conditions. In addition, the results show that ANOVA proved a good accordance between the experimental and predicted values with acceptable correlation coefficients ($R^2 = 0.9541$ and $R^2 = 0.9456$ adjusted) for naphthalene (NAP) removal. Yaqubzadeh et al. [59] studied naphthalene removal from aqueous solution by facile synthesis of silica aerogel using RSM. Their input parameters were Time, pH, and adsorbent dosages at a fixed naphthalene concentration of 34 mg·mL^{-1}. They obtained a second-order nonlinear model for predicting naphthalene removal that was reported according to the ANOVA analysis. The optimum conditions were a time of 120 min, pH 4, and an adsorbate dosage of 4 g·L^{-1}. The results show that the adequacy of the model was guaranteed by evaluating statistical factors including determination coefficient ($R^2 = 0.903$), adjusted R^2 (0.877), and sufficient accuracy (19.23).

Despite several studies on naphthalene removal by novel adsorbents, to the authors' knowledge, there has not been any application of the IRMOF-3 for naphthalene adsorbent. In this study, the adsorption rate of naphthalene by porous IRMOF-3 nanostructure has been investigated and the impact of naphthalene concentration, pH, time, and adsorbent dose as independent variables on removal percentage are studied. In order for the studied parameters to be at equal distances, the value of α in this study is set to 1.

2. Materials and Methods

2.1. Materials

Zinc nitrate haxahydrate and 2-aminoterephthalic acid were purchased from Sigma Aldrich. Naphthalene crystalline powder C$_{10}$H$_8$, N,N-dimethylformamid, and ethanol were supplied from Merck, Scharlau, and Zakaria Jahrom, respectively. All materials are more than 99.9% pure and used as supplied.

2.2. IRMOF-3 Synthesis

IRMOF-3 was obtained according to the procedure described elsewhere [60] with slight modification. In brief, zinc nitrate hexahydrate (1.2 g, 4.59 mmol) and 2-aminoterephthalic acid (0.3 g, 1.66 mmol) were dissolved in dry DMF (30 mL). The obtained suspension was stirred for 20 min at room temperature. This mixture was then stored in an oven for 24 h at 105 °C, followed by a slow cooling to room temperature. The solvent was removed and the brown crystals were rinsed 3 times with dry DMF. The products were then immersed in CHCl$_3$ for three days, the solvent was replaced daily with a fresh one. Finally, the solvent was decanted and the resulting brown powder was dried at 120 °C.

2.3. IRMOF-3 Characterization

NanoSpec2 UV-Vis Spectrophotometer (Nanolytik, EMCLAB, Duisburg, Germany), X-ray diffraction (XRD) (MPD 3000, Novara, Italy—G. N. R. Analytical Instruments Group), Fourier-transform infrared spectroscopy (FTIR) Spectrometer (RX-I, PerkinElmer, Waltham, MA, USA), scanning electron microscopy (SEM) (Leo1430VP, Carl Zeiss AG, Jena, Germany), thermo gravimetric analysis (TGA) (PT-1000, Linseis STA, Selb, Germany), and Brunauer–Emmett–Teller (BET) (BELSORP miniII, Microtrac, Japan) were used to analyze samples.

2.4. Sample Preparation and Adsorption Characterization

A pH meter (F470, Qis, United States), an ultrasonic bath homogenizer (PARSONIC 11s), and a laboratory-scale centrifuge (Sahand T.A., Iran) were used for sample preparation. A stock solution of 50 mg·L^{-1} of naphthalene was prepared in water–ethanol (30:70% v/v) and later used to prepare solutions with concentrations of 15, 20, 25, 30, 35, 40, 45 and 50 mg·L^{-1}. To regulate the pH of the solutions, hydrochloric acid (0.1 M) and sodium hydroxide (0.1 M) were used. The samples were placed in a shaker operating at 500 rpm for proper mixing of the adsorbent and the adsorbate. An ultrasonic bath was then used for homogenization and, after a certain time, the adsorbent was removed by centrifugation and the residual naphthalene concentration was analyzed using a spectrophotometer at a wavelength of 220 nm. The percentage of naphthalene removal and its adsorption value (mg·g^{-1}) were calculated by Equations (1) and (2), respectively:

$$R\% = \frac{\left(C_0 - C_f\right)}{C_0} \times 100 \tag{1}$$

$$q_e = \frac{\left(C_0 - C_f\right) \times v}{w} \tag{2}$$

In these relations, C_0 and C_f indicate the initial and final concentration of naphthalene (mg·L^{-1}). In addition, w is the adsorbent dosage (g) and v is the volume of solution (L).

2.5. Experimental Design Method

RSM was used to optimize the adsorption process. RSM is a well-organized and economical method that employs a set of mathematical and statistical approaches for analyzing the effect of several independent parameters on the response and adaptation of experimental models for experimental data. RSM outcome depends on the appropriateness of experimental polynomial models [61]. RSM minimizes the experimentation [62]. RSM is categorized as CCD, Box–Behnken design, and factorial design of three levels [63]. Among these, CCD is better suited for optimizing various operational parameters.

To evaluate the interplay of operational parameters A: pH (3–9), B: naphthalene concentration (15–50 mg·L^{-1}), C: contact time (30–60 min), and D: dose adsorbents (0.01–0.10 g·L^{-1}) in CCD are used as input variables, while their effect on removal percent of naphthalene by IRMOF-3 was considered as a response. In the CCD method for each variable highest level, high, center, low, and lowest, five levels + α, +1, 0, −1 and −α were selected (see Table 1). In total, 30 independent test runs were designed to systematically assess the potential impact of different operating conditions. In order to minimize possible experimental errors, all experimental designs were performed randomly. Then, to evaluate the contribution of the main factors and their interaction, analysis of variance (ANOVA) was used by Design Expert 7.0 software (95% confidence level) (see Table 2).

Table 1. Experimental variables and their levels in central composite design.

Independent Variables			Range and Levels (Coded)				
Factors	Coded	Units	−α	−1	0	+1	+α
pH	A		3	3	7	11	11
Concentration	B	mg·L^{-1}	15	15	32.5	50	50
Time	C	min	30	30	45	60	60
Adsorbent dose	D	g·L^{-1}	0.01	0.1	0.055	0.10	0.11

Table 2. Central composite design matrix with naphthalene adsorption experiments (%).

RUN	A: pH	B: Concentration (mg/L)	C: Time (min)	D: Adsorbent dose (g·L^{-1})	Adsorption %
1	7	32.5	45	0.06	44.15
2	3	15	30	0.1	49.01
3	11	15	30	0.1	52.81
4	3	32.5	45	0.06	40.15
5	3	50	30	0.01	21.08
6	3	15	30	0.01	42.27
7	3	50	60	0.1	40.21
8	7	32.5	45	0.06	44.15
9	11	50	60	0.1	45.96
10	11	50	30	0.1	33.01
11	11	15	30	0.01	46.1
12	11	32.5	45	0.06	43.11
13	11	50	60	0.01	31.63
14	3	50	30	0.1	21.08
15	7	32.5	30	0.06	38.23
16	7	50	45	0.06	37.5
17	11	50	30	0.01	28.13
18	11	15	60	0.01	56.6
19	7	15	45	0.06	47.4
20	7	32.5	45	0.01	33.12
21	3	50	60	0.01	25.87
22	7	32.5	45	0.06	44.15
23	3	15	60	0.01	51.31
24	7	32.5	45	0.06	44.15
25	7	32.5	45	0.1	48.91
26	7	32.5	45	0.06	44.15
27	3	15	60	0.1	61.73
28	11	15	60	0.1	80.96
29	7	32.5	45	0.06	44.15
30	7	32.5	60	0.06	46.71

The relationship between the independent parameters and the responses obtained by the quadratic polynomial model was expressed [64,65]. The model equation is presented as follows:

$$Y = \beta_0 + \sum_{i=1}^{k} \beta_i X_i + \sum_{i=1}^{k} \sum_{j=1}^{k} \beta_{ij} X_i X_j + \sum_{i=1}^{k} \beta_{ii} X_i^2 + \varepsilon \tag{3}$$

In Equation (3), Y is the predicted response (removal percent). X_i and X_j are encrypted values of independent variables. β_0 is the model constant. β_i, β_{ii} and β_{ij} are coefficients of regression for linear, quadratic, and interaction terms, respectively. k is expressed as the number of independent variables and ε is the remaining error of the model. The results of naphthalene adsorption are reported as an analysis of variance (ANOVA) and model outputs including three-dimensional diagrams, contour diagrams, and predicted diagrams against real values. In addition, sufficient accuracy (AP), regression coefficient (R^2), p value, and F value (Fisher variation ratio) were the essential parameters to confirm the relationship, importance, and appropriateness of the designed model.

3. Results and Discussion

3.1. IRMOF-3 Characterization

FT-IR analysis, depicted in Figure 1a, was utilized to investigate the structural characteristics of the IRMOF-3 sample. The peaks at 3219.33 and 3127.43 cm^{-1} are correlated with the asymmetric and symmetric stretching of amine groups, respectively [66]. Strong peaks at 1388.63 and 1569.36 cm^{-1} represent the symmetric and asymmetric vibrations of dicarboxylate O-C=O and C=C in the benzene ring, respectively [67]. A slight shift in the peaks is attributed to the hydrogen bonds formed with the primary amines and -OH belonging

to the carboxyl group of IRMOF-3. The strong band at 1243.75 cm^{-1} is dedicated to the C-N bond stretching vibrations. The aromatic C-H bending of the porous nanostructure can be seen at 1157.39 and 814.03 cm^{-1} [68]. To investigate the crystal characteristics of the IRMOF-3 sample, the XRD analysis, as depicted in Figure 1b, was used. The diffraction peaks at 2θ = 6.8, 9.8, and 13.8° correspond to (200), (220), and (400) planes, respectively. These diffraction peaks are consistent with the reported IRMOF-3 structure [69]. Finally, low-grade peaks confirm the formation of a crystalline structure as expected.
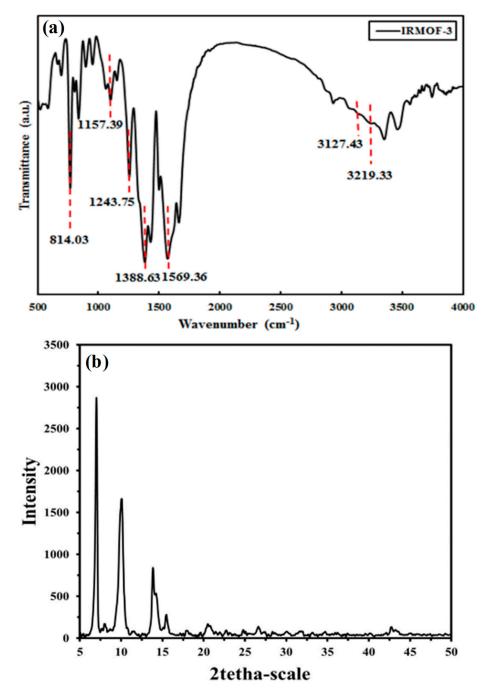
Figure 1. (**a**) FTIR spectrum and (**b**) XRD pattern of IRMOF-3 sample.

The SEM micrographs presented in Figure 2a,b are used to study the morphology and structure of the IRMOF-3 sample. The SEM images represent a well-formed cubic crystal structure of IRMOF-3. The results confirm that the synthesized porous nanostructure is morphologically similar to the previous reports [70].
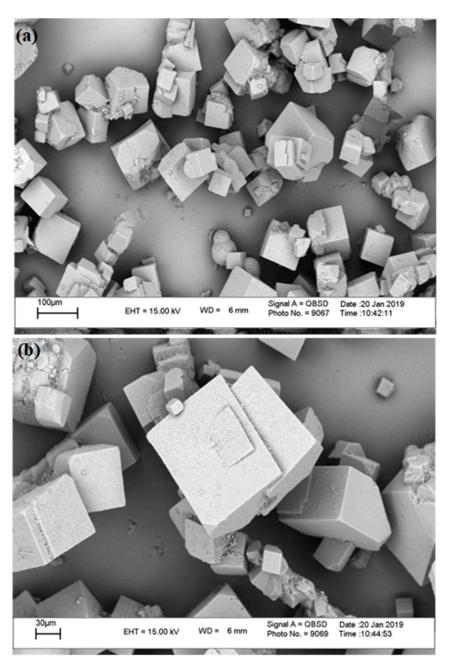
Figure 2. SEM images of IRMOF−3 (**a**,**b**).

In order to evaluate the porosity of the IRMOF-3 sample, the nitrogen adsorption–desorption isotherms analysis (BET) was performed as shown in Figure 3. The IRMOF-3 adsorption isotherms have type IV characteristics. According to Table 3, BET-specific surface area, pore volume, and pore diameter of the IRMOF-3 sample are 718.11 $m^2 \cdot g^{-1}$, 0.378 cm^3/g, and 2.105 nm, respectively. Thus, the samples have mesoporous features. Comparison of the Specific surface area of IRMOF-3 with other adsorbents and their naphthalene adsorption efficiency are summarized in Table 4.
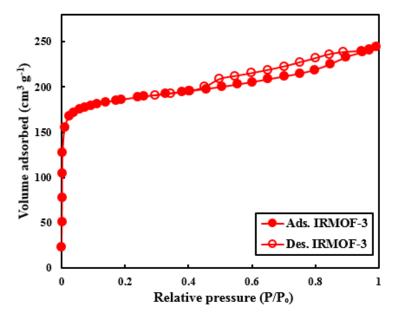
Figure 3. BET diagram of IRMOF-3.

Table 3. Physical properties of IRMOF-3 porous nanostructure.

Sample	Specific Area (m^2/g)	Pore Volume (cm^3/g)	Pore Diameter (nm)
IRMOF-3	718.11	0.378	2.105

Table 4. Comparison of Specific area (m^2/g) for IRMOF-3 with other adsorbents regarding naphthalene absorption efficiency.

Adsorbent	Specific Area ($m^2 \cdot g^{-1}$)	PAHs	Adsorption Efficiency	Ref.
ZIF-8	1299	Acenaphthene	60.7%	[71]
NH_2-UiO-66(Zr)	985	Naphthalene	97.7%	[72]
green mCS/GO	22.8358	Naphthalene	70%	[73]
Fe@N-L-GM	10.16	Naphthalene	97.81%	[74]
CuZnFeAlO	125	Naphthalene	90.1%	[75]
IRMOF-3	718.11	Naphthalene	80.96	This study

Figure 4 shows the TGA and DTG curves of the IRMOF-3 sample under the nitrogen atmosphere. According to Figure 4, by increasing temperature from 30 to 115 °C, 2% weight loss occurs. This weight loss is related to the release of adsorbed water molecules on the surface and pores of the sample. Increasing temperature from 115 °C to 321 °C results in 7% weight loss which can be due to the release of DMF molecules on the MOF cavities as well as the degradation of the unreacted 2-amino terephthalic acids trapped inside the MOF cavities [68]. From 321 °C to 550 °C, a sharp weight loss of about 38% is observed, which can be due to thermal degradation of the organic linkers or 2-amino terephthalic acid in the IRMOF-3 structure. On the other hand, the approximate constant slope of the TGA curve of the sample after 490 °C represents the thermal stability of the material left after the degradation process. The residual weight of the sample at the end of heat degradation up to 550 °C is about 52%, which is related to the weight of remaining organic ash and stable forms of ZnO.
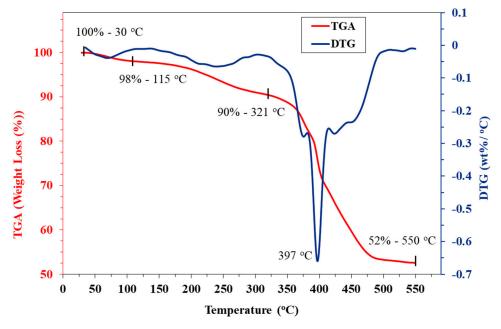
Figure 4. TGA results of IRMOF-3 porous nanostructures.

3.2. Model Analysis Based on CCD

CCD is applied for assessing the fitness of the obtained quadratic model, which identifies the interplay of operational variables and their influence on the absorption (%). The fitting of the mathematical and experimental model and analysis of experimental data of naphthalene adsorption was performed using analysis of variance (ANOVA) and the statistical summary of the quadratic model is expressed in (Table 5). An important correlation between dependent variables and obtained responses for naphthalene removal is expressed in Equation (4).

$$\text{Adsorption (\%)} = +42.93 + 3.64A - 11.32B + 6.07C + 5.42D - 0.10AB - 1.25BC - 0.92BD + 2.82CD - 9.516 \times 10^{-3} B^2 + 0.010C^2 \tag{4}$$

Table 5. Analysis of variance (ANOVA) for naphthalene removal (%).

Response	1	Absorption			
ANOVA for Response Surface Reduced Quadratic Model					
Analysis of variance table [Partial sum of squares—Type III]					
	Sum of		Mean	F	p-value
Source	Squares	df	Square	Value	Prob > F
Model	3902.805	10	390.2805	30.74218738	<0.0001	significant
A-pH	239.0756	1	239.0756	18.83185395	0.0004
B-Concentration	2305.658	1	2305.658	181.6154259	<0.0001
C-time	663.2082	1	663.2082	52.24055604	<0.0001
D-Absorbent dose	528.8836	1	528.8836	41.65987941	<0.0001
AB	0.172225	1	0.172225	0.013566071	0.9085
BC	25.1001	1	25.1001	1.977121484	0.1758
BD	13.4689	1	13.4689	1.060938066	0.3159
CD	127.2384	1	127.2384	10.02250088	0.0051
B^2	0.000312	1	0.000312	2.46×10^{-5}	0.9961
C^2	0.000379	1	0.000379	2.98×10^{-5}	0.9957
Residual	241.2102	19	12.69527		
Lack of Fit	241.2102	14	17.2293		

Table 5. *Cont.*

Response	1	Absorption	
Pure Error	0	5	0
Cor Total	4144.015	29	
Std. Dev.	3.563043	R^2	0.941793
Mean	42.92633	Adj R^2	0.911158
C.V. %	8.300366	Pred R^2	0.815208
PRESS	765.781	Adeq Precision	24.52136

Clearly, naphthalene adsorption percentage is a function of A, B, C, Dm AB, BC, BD, CD, B^2, and C^2. Recall that A, B, C, and D represent the pH of the solution, naphthalene concentration, contact time and dosage of adsorbent, respectively. The results of ANOVA illustrated that the quadratic model remarkably expresses the variables' response and interaction. Large F value (30.74) and small *p*-value ($p < 0.0001$) prove that the quadratic model is very appropriate to the insignificance of B^2 and C^2 (low F-value and $p < 0.05$). The quadratic model is further compared and complies with the findings of other studies on naphthalene adsorption [57,76–78]. The accuracy and validity of the experimental responses are investigated using sufficient accuracy, variance coefficient (C.V.%), regression coefficient and standard deviation. A reliable and repeatable model must have a C.V. less than 10% [79]. The C.V. value in this study is 8.30%. "Coefficient of determination (R^2)" and "adjusted coefficient (R^2-adjusted)" in this study are 0.9418 and 0.9112, respectively. Comparative values of R^2 and R^2-adjusted indicate that the test data are very suitable in the quadratic model. The observed experimental responses (% adsorption) match the predicted value of the confirmed model with the value of R^2.

Figure 5 shows the linear correlation between the actual experimental response and the predicted response to the percentage of naphthalene uptake. This linear correlation demonstrates that the actual experimental values of naphthalene adsorption are in good agreement with the predicted value of the model. The quadratic model well describes the experimental data.
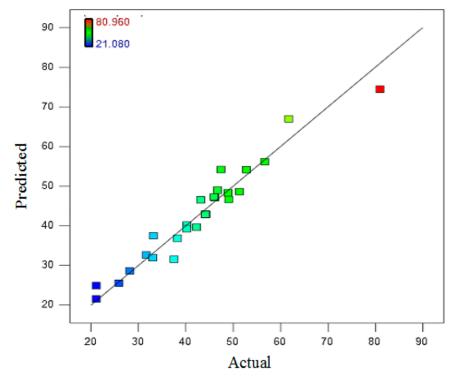

Figure 5. The diagram of predicted and actual values for the adsorption of naphthalene on IRMOF-3.

3.3. Impact of Combination of Variables on Response Levels

Response level plots are a more suitable tool for investigating the significant effects and interactions of two parameters keeping all other parameters at the central levels [80,81]. The effects of concentration–contact time, concentration–adsorbent amount, contact time–adsorbent amount and pH–concentration on the removal percentage of naphthalene were determined and the results are depicted as 3D curves of the response surface in Figure 6. The combined effect of contact time–concentration on naphthalene removal is shown in Figure 6a. Naphthalene uptake percentage increased with decreasing its concentration and increasing contact time. This may be owing to the availability of ample surface-active sites of the porous IRMOF-3 nanostructure per naphthalene molecule. At high naphthalene concentrations, the active sites of the porous nanostructure are rapidly filled with naphthalene molecules. Longer contact time enhances the opportunity for naphthalene molecules to effectively interact with the active sites. At high naphthalene concentration and/or low contact time enhanced competition between naphthalene molecules and/or reduced effective naphthalene molecules-MOF active sites interaction reduces the naphthalene uptake by MOF.
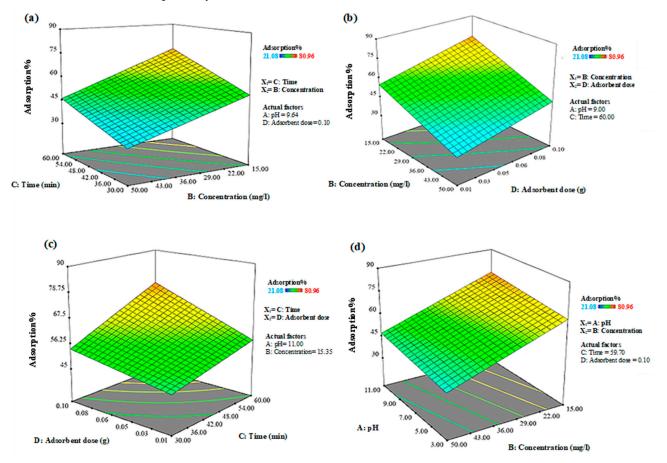

Figure 6. Typical 3D response surface plots for the interaction of variables in response: (**a**) time–naphthalene concentration, (**b**) adsorbent dose–naphthalene concentration, (**c**) adsorbent dose–time, and (**d**) pH–naphthalene concentration.

It can be seen from Figure 6b that adsorption % improves with decreasing naphthalene concentration and/or increasing adsorbent amount. Increasing the ratio of adsorbent/naphthalene concentration increases the number of active sites per naphthalene molecule which in turn enhances the probability of effective naphthalene molecules-MOF active sites interaction which is positively correlated with the adsorption percentage.

Figure 6c shows that with the increase in time and/or adsorbent dosage, the absorption percentage increases. As mentioned earlier, by increasing the adsorbent dosage the number

of active sites available for adsorption increases [82]. The same explanation of the time effect explained in Figure 6a is also valid for Figure 6c. The influence of pH and naphthalene concentration on naphthalene removal is reported in Figure 6d. IRMOF-3 here acts as a dual-site adsorbent. The alkaline properties of MOFs are due to the presence of the free amine groups and the acidity of these compounds is attributed to the Zn-OH groups as well as the presence of structural defects. Thus, as naphthalene possesses a negative surface charge in the alkaline medium [83], it can chemically interact with the adsorbent Zn-OH groups at higher pH values. This can justify the significant increase in the adsorption capacity with the increasing pH.

4. Conclusions

In this work, IRMOF-3 was successfully synthesized and characterized by FT-IR, XRD, SEM, TGA, and BET analysis. The adsorbent was then utilized for naphthalene removal from a water–ethanol solution (30:70% v/v). To obtain the optimum adsorption condition, the CCD approach was utilized with a total of 30 independent experiments. It was found that the optimal IRMOF-3 adsorbability occurs at 15 mg·L^{-1} of naphthalene concentration, pH = 11, contact time of 60 min, and 0.1 g·L^{-1} of adsorbent dose, respectively. The results indicate that at high naphthalene concentrations, the active sites of the porous MOF nanostructure are rapidly filled which reduces the percentage of adsorption. Longer contact time provides a better opportunity for naphthalene interaction with the surface-active sites. The adsorption percentage increases with increasing adsorbent dose due to the availability of a larger number of adsorption sites. The obtained results suggest that IRMOF-3 acts as a dual-site adsorbent. The alkaline properties of MOFs are owing to the presence of the free amine groups and the acidity of these compounds is attributed to the Zn-OH groups as well as the presence of structural defects. On the other hand, naphthalene polarity enhances its chemical interaction with the adsorbent Zn-OH groups at higher pH values. This can justify the significant increase in the adsorption capacity with the increasing pH. This study revealed that IRMOF-3 is an efficient adsorbent which can be utilized for naphthalene removal from contaminated water.

References

1. Montgomery, M.A.; Elimelech, M. Water And Sanitation in Developing Countries: Including Health in the Equation. *Environ. Sci. Technol.* **2007**, *41*, 17–24. [CrossRef] [PubMed]
2. Shannon, M.A.; Bohn, P.W.; Elimelech, M.; Georgiadis, J.G.; Marinas, B.J.; Mayes, A.M. Science and technology for water purification in the coming decades. *Nanosci. Technol. A Collect. Rev. Nat. J.* **2010**, *452*, 337–346.
3. Qiu, J. China faces up to groundwater crisis. *Nature* **2010**, *466*, 308. [CrossRef]
4. Alipour, A.; Kalashgarani, M.Y. Nano Protein and Peptides for Drug Delivery and Anticancer Agents. *Adv. Appl. NanoBio-Technol.* **2022**, *3*, 60–64.
5. Mousavi, S.M.; Hashemi, S.A.; Rahmanian, V.; Kalashgrani, M.Y.; Gholami, A.; Omidifar, N.; Chiang, W.-H. Highly Sensitive Flexible SERS-Based Sensing Platform for Detection of COVID-19. *Biosensors* **2022**, *12*, 466. [CrossRef]
6. Shah, A.; Shahzad, S.; Munir, A.; Nadagouda, M.; Khan, G.S.; Shams, D.F.; Dionysiou, D.D.; Rana, U.A. Micelles as Soil and Water Decontamination Agents. *Chem. Rev.* **2016**, *116*, 6042–6074. [CrossRef]
7. Kalashgarani, M.Y.; Babapoor, A. Application of nano-antibiotics in the diagnosis and treatment of infectious diseases. *Adv. Appl. NanoBio-Technol.* **2022**, *3*, 22–35.

8. Mousavi, S.M.; Hashemi, S.A.; Kalashgrani, M.Y.; Gholami, A.; Omidifar, N.; Babapoor, A.; Rao, N.V.; Chiang, W.-H. Recent Advances in Plasma-Engineered Polymers for Biomarker-Based Viral Detection and Highly Multiplexed Analysis. *Biosensors* **2022**, *12*, 286. [CrossRef]

9. Parales, R.E.; Lee, K.; Resnick, S.M.; Jiang, H.; Lessner, D.J.; Gibson, D.T. Substrate Specificity of Naphthalene Dioxygenase: Effect of Specific Amino Acids at the Active Site of the Enzyme. *J. Bacteriol.* **2000**, *182*, 1641–1649. [CrossRef]

10. Mousavi, S.M.; Hashemi, S.A.; Kalashgrani, M.Y.; Omidifar, N.; Bahrani, S.; Rao, N.V.; Babapoor, A.; Gholami, A.; Chiang, W.-H. Bioactive Graphene Quantum Dots Based Polymer Composite for Biomedical Applications. *Polymers* **2022**, *14*, 617. [CrossRef]

11. Goel, R.K.; Flora, J.R.; Ferry, J. Mechanisms for naphthalene removal during electrolytic aeration. *Water Res.* **2003**, *37*, 891–901. [CrossRef] [PubMed]

12. Mousavi, S.M.; Hashemi, S.A.; Kalashgrani, M.Y.; Omidifar, N.; Lai, C.W.; Rao, N.V.; Gholami, A.; Chiang, W.-H. The Pivotal Role of Quantum Dots-Based Biomarkers Integrated with Ultra-Sensitive Probes for Multiplex Detection of Human Viral Infections. *Pharmaceuticals* **2022**, *15*, 880. [CrossRef]

13. Agah, M.; Binazadeh, M.; Baghulifard, N.; Sarani, M. Demulsification of saline-in-crude oil via biocompatible cellulose derivative polymers. *Fuel* **2022**, *311*, 122533. [CrossRef]

14. Ania, M.C.O.; Cabal, B.; Parra, J.B.; Pis, J.J. Importance of the Hydrophobic Character of Activated Carbons on the Removal of Naphthalene from the Aqueous Phase. *Adsorpt. Sci. Technol.* **2007**, *25*, 155–167. [CrossRef]

15. Mousavi, S.M.; Hashemi, S.A.; Kalashgrani, M.Y.; Kurniawan, D.; Gholami, A.; Rahmanian, V.; Omidifar, N.; Chiang, W.-H. Recent Advances in Inflammatory Diagnosis with Graphene Quantum Dots Enhanced SERS Detection. *Biosensors* **2022**, *12*, 461. [CrossRef] [PubMed]

16. Law, A.M.J.; Aitken, M.D. Bacterial Chemotaxis to Naphthalene Desorbing from a Nonaqueous Liquid. *Appl. Environ. Microbiol.* **2003**, *69*, 5968–5973. [CrossRef] [PubMed]

17. Amani, A.M.; Hashemi, S.A.; Mousavi, S.M.; Pouya, H.; Arash, V. Electric Field Induced Alignment of Carbon Nanotubes: Methodology and Outcomes. In *Carbon Nanotubes-Recent Progress*; IntechOpen: London, UK, 2017.

18. Mousavi, S.M.; Hashemi, S.A.; Kalashgrani, M.Y.; Rahmanian, V.; Gholami, A.; Chiang, W.-H.; Lai, C.W. Biomedical Applications of an Ultra-Sensitive Surface Plasmon Resonance Biosensor Based on Smart MXene Quantum Dots (SMQDs). *Biosensors* **2022**, *12*, 743. [CrossRef]

19. Ashour, I.; Abu Al-Rub, F.A.; Sheikha, D.; Volesky, B. Biosorption of Naphthalene from Refinery Simulated Waste-Water on Blank Alginate Beads and Immobilized Dead Algal Cells. *Sep. Sci. Technol.* **2008**, *43*, 2208–2224. [CrossRef]

20. Mousavi, S.M.; Hashemi, S.A.; Kalashgrani, M.Y.; Kurniawan, D.; Gholami, A.; Chiang, W.-H. Bioresource-Functionalized Quantum Dots for Energy Generation and Storage: Recent Advances and Feature Perspective. *Nanomaterials* **2022**, *12*, 3905. [CrossRef]

21. Nesterenko-Malkovskaya, A.; Kirzhner, F.; Zimmels, Y.; Armon, R. Eichhornia crassipes capability to remove naphthalene from wastewater in the absence of bacteria. *Chemosphere* **2012**, *87*, 1186–1191. [CrossRef]

22. Mousavi, S.M.; Hashemi, S.A.; Gholami, A.; Kalashgrani, M.Y.; Rao, N.V.; Omidifar, N.; Hsiao, W.W.-W.; Lai, C.W.; Chiang, W.-H. Plasma-Enabled Smart Nanoexosome Platform as Emerging Immunopathogenesis for Clinical Viral Infection. *Pharmaceutics* **2022**, *14*, 1054. [CrossRef] [PubMed]

23. Binazadeh, M.; Karimi, I.A.; Li, Z. Fast biodegradation of long chain n-alkanes and crude oil at high concentrations with Rhodococcus sp. Moj-3449. *Enzym. Microb. Technol.* **2009**, *45*, 195–202. [CrossRef]

24. Aguilar, C.M.; Rodríguez, J.L.; Chairez, I.; Tiznado, H.; Poznyak, T. Naphthalene degradation by catalytic ozonation based on nickel oxide: Study of the ethanol as cosolvent. *Environ. Sci. Pollut. Res.* **2017**, *24*, 25550–25560. [CrossRef] [PubMed]

25. Srivastava, P.; Sreekrishnan, T.R.; Nema, A.K. Degradation of Low-Molecular-Weight PAHs: Naphthalene, Acenaphthylene, Phenanthrene, and Fluorene. *J. Hazardous, Toxic, Radioact. Waste* **2017**, *21*, 04017008. [CrossRef]

26. Wang, C.; Ma, L.; Liu, B.; Zhang, D.; Pan, B. Co-contaminant effects on ofloxacin adsorption onto activated carbon, graphite, and humic acid. *Environ. Sci. Pollut. Res.* **2017**, *24*, 23834–23842. [CrossRef] [PubMed]

27. Jiménez, S.; Andreozzi, M.; Micó, M.M.; Alvarez, M.G.; Contreras, S. Produced water treatment by advanced oxidation processes. *Sci. Total. Environ.* **2019**, *666*, 12–21. [CrossRef]

28. Hashemi, S.A.; Mousavi, S.M. Effect of bubble based degradation on the physical properties of Single Wall Carbon Nanotube/Epoxy Resin composite and new approach in bubbles reduction. *Compos. Part A Appl. Sci. Manuf.* **2016**, *90*, 457–469. [CrossRef]

29. da Silva, C.M.; Rocha, Q.D.C.; Rocha, P.C.S.; Louvisse, A.M.T.; Lucas, E.F. Removal of naphthalene from aqueous systems by poly(divinylbenzene) and poly(methyl methacrylate-divinylbenzene) resins. *J. Environ. Manag.* **2015**, *157*, 205–212. [CrossRef]

30. Karri, R.R.; Sahu, J. Modeling and optimization by particle swarm embedded neural network for adsorption of zinc (II) by palm kernel shell based activated carbon from aqueous environment. *J. Environ. Manag.* **2018**, *206*, 178–191. [CrossRef]

31. Mousavi, S.M.; Hashemi, S.A.; Esmaeili, H.; Amani, A.M.; Mojoudi, F. Synthesis of Fe3O4 Nanoparticles Modified by Oak Shell for Treatment of Wastewater Containing Ni(II). *Acta Chim. Slov.* **2018**, *65*, 750–756. [CrossRef] [PubMed]

32. Owabor, C.; Agarry, S.; Jato, D. Removal of naphthalene from aqueous system using unripe orange peel as adsorbent: Effects of operating variables. *Desalination Water Treat.* **2012**, *48*, 315–319. [CrossRef]

33. Younker, J.M.; Walsh, M.E. Impact of salinity and dispersed oil on adsorption of dissolved aromatic hydrocarbons by activated carbon and organoclay. *J. Hazard. Mater.* **2015**, *299*, 562–569. [CrossRef]

34. Kim, J.; Hyun, S. Sorption of ionic and nonionic organic solutes onto giant Miscanthus-derived biochar from methanol-water mixtures. *Sci. Total. Environ.* **2018**, *615*, 805–813. [CrossRef] [PubMed]

35. Seyed, M.M. Unsaturated polyester resins modified with cresol novolac epoxy and silica nanoparticles: Processing and mechanical properties. *Int. J. Chem. Pet. Sci. (IJCPS)* **2016**, *5*, 13–26.

36. Yang, Y.; Zhang, C.; Hu, Z. Impact of metallic and metal oxide nanoparticles on wastewater treatment and anaerobic digestion. *Environ. Sci. Process. Impacts* **2013**, *15*, 39–48. [CrossRef] [PubMed]

37. Ghaedi, M.; Daneshyar, A.; Asfaram, A.; Purkait, M.K. Adsorption of naphthalene onto high-surface-area nanoparticle loaded activated carbon by high performance liquid chromatography: Response surface methodology, isotherm and kinetic study. *RSC Adv.* **2016**, *6*, 54322–54330. [CrossRef]

38. Bayazit, Ş.S.; Yildiz, M.; Aşçi, Y.S.; Şahin, M.; Bener, M.; Eğlence, S.; Salam, M.A. Rapid adsorptive removal of naphthalene from water using graphene nanoplatelet/MIL-101 (Cr) nanocomposite. *J. Alloy. Compd.* **2017**, *701*, 740–749. [CrossRef]

39. Mousavi, S.M.; Hashemi, S.A.; Amani, A.M.; Saed, H.; Jahandideh, S.; Mojoudi, F. Polyethylene Terephthalate/Acryl Butadiene Styrene Copolymer Incorporated with Oak Shell, Potassium Sorbate and Egg Shell Nanoparticles for Food Packaging Applications: Control of Bacteria Growth, Physical and Mechanical Properties. *Polym. Renew. Resour.* **2017**, *8*, 177–196. [CrossRef]

40. Wang, X.-S.; Liang, J.; Li, L.; Lin, Z.-J.; Bag, P.P.; Gao, S.-Y.; Huang, Y.-B.; Cao, R. An Anion Metal–Organic Framework with Lewis Basic Sites-Rich toward Charge-Exclusive Cationic Dyes Separation and Size-Selective Catalytic Reaction. *Inorg. Chem.* **2016**, *55*, 2641–2649. [CrossRef]

41. Czaja, A.U.; Trukhan, N.; Müller, U. Industrial applications of metal–organic frameworks. *Chem. Soc. Rev.* **2009**, *38*, 1284–1293. [CrossRef]

42. Azhdari, R.; Mousavi, S.M.; Hashemi, S.A.; Bahrani, S.; Ramakrishna, S. Decorated graphene with aluminum fumarate metal organic framework as a superior non-toxic agent for efficient removal of Congo Red dye from wastewater. *J. Environ. Chem. Eng.* **2019**, *7*, 103437. [CrossRef]

43. Yabushita, M.; Li, P.; Bernales, V.; Kobayashi, H.; Fukuoka, A.; Gagliardi, L.; Farha, O.K.; Katz, A. Unprecedented selectivity in molecular recognition of carbohydrates by a metal–organic framework. *Chem. Commun.* **2016**, *52*, 7094–7097. [CrossRef]

44. Mousavi, S.; Aghili, A.; Hashemi, S.; Goudarzian, N.; Bakhoda, Z.; Baseri, S. Improved Morphology and Properties of Nanocomposites, Linear Low Density Polyethylene, Ethylene-Co-Vinyl Acetate and Nano Clay Particles by Electron Beam. *Polym. Renew. Resour.* **2016**, *7*, 135–153. [CrossRef]

45. Binazadeh, M. Cellulose derivative polymers for demulsification of lagoon wastewater-in-crude oil systems: An efficient water reuse strategy. *J. Pet. Sci. Eng.* **2022**, *211*, 110120. [CrossRef]

46. Eddaoudi, M.; Kim, J.; Rosi, N.; Vodak, D.; Wachter, J.; O'Keeffe, M.; Yaghi, O.M. Systematic Design of Pore Size and Functionality in Isoreticular MOFs and Their Application in Methane Storage. *Science* **2002**, *295*, 469–472. [CrossRef] [PubMed]

47. Mousavi, S.M.; Esmaeili, H.; Arjmand, O.; Karimi, S.; Hashemi, S.A. Biodegradation Study of Nanocomposites of Phenol Novolac Epoxy/Unsaturated Polyester Resin/Egg Shell Nanoparticles Using Natural Polymers. *J. Mater.* **2015**, *2015*, 1–6. [CrossRef]

48. Burgoyne, A.; Meijboom, R. Knoevenagel Condensation Reactions Catalysed by Metal-Organic Frameworks. *Catal. Lett.* **2013**, *143*, 563–571. [CrossRef]

49. Mousavi, S.M.; Zarei, M.; Hashemi, S.A.; Ramakrishna, S.; Chiang, W.-H.; Lai, C.W.; Gholami, A.; Omidifar, N.; Shokripour, M. Asymmetric Membranes: A Potential Scaffold for Wound Healing Applications. *Symmetry* **2020**, *12*, 1100. [CrossRef]

50. Chang, C.-Y.; Lee, C.-L.; Pan, T.-M. Statistical optimization of medium components for the production of Antrodia cinnamomea AC0623 in submerged cultures. *Appl. Microbiol. Biotechnol.* **2006**, *72*, 654–661. [CrossRef]

51. Mousavi, S.M.; Hashemi, S.A.; Ramakrishna, S.; Esmaeili, H.; Bahrani, S.; Koosha, M.; Babapoor, A. Green synthesis of supermagnetic Fe3O4–MgO nanoparticles via Nutmeg essential oil toward superior anti-bacterial and anti-fungal performance. *J. Drug Deliv. Sci. Technol.* **2019**, *54*, 101352. [CrossRef]

52. Binazadeh, M.; Li, Z.; Karimi, I.A. Optimization of Biodegradation of Long Chain n-Alkanes by Rhodococcus sp. Moj-3449 Using Response Surface Methodology. *Phys. Chem. Res.* **2020**, *8*, 45–59.

53. Chakravarti, R.; Sahai, V. Optimization of compactin production in chemically defined production medium by Penicillium citrinum using statistical methods. *Process. Biochem.* **2002**, *38*, 481–486. [CrossRef]

54. Mousavi, S.; Arjmand, O.; Hashemi, S.; Banaei, N. Modification of the Epoxy Resin Mechanical and Thermal Properties with Silicon Acrylate and Montmorillonite Nanoparticles. *Polym. Renew. Resour.* **2016**, *7*, 101–113. [CrossRef]

55. Arizavi, A.; Mirbagheri, N.S.; Hosseini, Z.; Chen, P.; Sabbaghi, S. Efficient removal of naphthalene from aqueous solutions using a nanoporous kaolin/Fe3O4 composite. *Int. J. Environ. Sci. Technol.* **2019**, *17*, 1991–2002. [CrossRef]

56. Farzadkia, M.; Ghorbanian, M.; Biglari, H.; Gholami, M.; Mehrizi, E.A. Application of the central composite design to optimization of petroleum hydrocarbons removal from oilfield water using advanced oxidation process. *Arch. Environ. Prot.* **2018**, *44*, 22–30.

57. Borousan, F.; Yousefi, F.; Ghaedi, M. Removal of malachite green dye using IRMOF-3–MWCNT-OH–Pd-NPs as a novel adsorbent: Kinetic, isotherm, and thermodynamic studies. *J. Chem. Eng. Data* **2019**, *64*, 4801–4814. [CrossRef]

58. Rani, C.N.; Karthikeyan, S. Investigation of Naphthalene Removal from Aqueous Solutions in an Integrated Slurry Photocatalytic Membrane Reactor: Effect of Operating Parameters, Identification of Intermediates, and Response Surface Approach. *Polycycl. Aromat. Compd.* **2021**, *41*, 805–824. [CrossRef]

59. Yaqubzadeh, A.; Ahmadpour, A.; Bastami, T.R.; Hataminia, M. Low-cost preparation of silica aerogel for optimized adsorptive removal of naphthalene from aqueous solution with central composite design (CCD). *J. Non-Crystalline Solids* **2016**, *447*, 307–314. [CrossRef]

60. Sá, J.; Szlachetko, J.; Kleymenov, E.; Lothschütz, C.; Nachtegaal, M.; Ranocchiari, M.; Safonova, O.V.; Servalli, M.; Smolentsev, G.; van Bokhoven, J.A. Fine tuning of gold electronic structure by IRMOF post-synthetic modification. *RSC Adv.* **2013**, *3*, 12043–12048. [CrossRef]

61. Bezerra, M.A.; Santelli, R.E.; Oliveira, E.P.; Villar, L.S.; Escaleira, L.A. Response surface methodology (RSM) as a tool for optimization in analytical chemistry. *Talanta* **2008**, *76*, 965–977. [CrossRef]

62. Jain, M.; Garg, V.; Kadirvelu, K. Investigation of Cr(VI) adsorption onto chemically treated Helianthus annuus: Optimization using Response Surface Methodology. *Bioresour. Technol.* **2011**, *102*, 600–605. [CrossRef] [PubMed]

63. Mazaheri, H.; Ghaedi, M.; Asfaram, A.; Hajati, S. Performance of CuS nanoparticle loaded on activated carbon in the adsorption of methylene blue and bromophenol blue dyes in binary aqueous solutions: Using ultrasound power and optimization by central composite design. *J. Mol. Liq.* **2016**, *219*, 667–676. [CrossRef]

64. Kataria, N.; Garg, V. Optimization of Pb (II) and Cd (II) adsorption onto ZnO nanoflowers using central composite design: Isotherms and kinetics modelling. *J. Mol. Liq.* **2018**, *271*, 228–239. [CrossRef]

65. Dashamiri, S.; Ghaedi, M.; Asfaram, A.; Zare, F.; Wang, S. Multi-response optimization of ultrasound assisted competitive adsorption of dyes onto Cu (OH)2-nanoparticle loaded activated carbon: Central composite design. *Ultrason. Sonochem.* **2017**, *34*, 343–353. [CrossRef]

66. Zhao, M.; Deng, K.; He, L.; Liu, Y.; Li, G.; Zhao, H.; Tang, Z. Core–Shell Palladium Nanoparticle@Metal–Organic Frameworks as Multifunctional Catalysts for Cascade Reactions. *J. Am. Chem. Soc.* **2014**, *136*, 1738–1741. [CrossRef] [PubMed]

67. Kumar, A.; Chowdhuri, A.R.; Kumari, A.; Sahu, S.K. IRMOF-3: A fluorescent nanoscale metal organic frameworks for selective sensing of glucose and Fe (III) ions without any modification. *Mater. Sci. Eng. C* **2018**, *92*, 913–921. [CrossRef]

68. Nuri, A.; Vucetic, N.; Smått, J.-H.; Mansoori, Y.; Mikkola, J.-P.; Murzin, D.Y. Pd Supported IRMOF-3: Heterogeneous, Efficient and Reusable Catalyst for Heck Reaction. *Catal. Lett.* **2019**, *149*, 1941–1951. [CrossRef]

69. Rather, R.A.; Siddiqui, Z.N. Sulfonic acid functionalized metal–organic framework (S-IRMOF-3): A novel catalyst for sustainable approach towards the synthesis of acrylonitriles. *RSC Adv.* **2019**, *9*, 15749–15762. [CrossRef]

70. Rostamnia, S.; Morsali, A. Size-controlled crystalline basic nanoporous coordination polymers of Zn4O(H2N-TA)3: Catalytically study of IRMOF-3 as a suitable and green catalyst for selective synthesis of tetrahydro-chromenes. *Inorganica Chim. Acta* **2014**, *411*, 113–118. [CrossRef]

71. Zango, Z.U.; Ramli, A.; Jumbri, K.; Abdurrahman, M. UiO-66 and ZIF-8 Metal-organic Frameworks for Acenaphthene Adsorption. In Proceedings of the 6th International Conference on Fundamental and Applied Sciences: ICFAS 2020, Kuching, Malaysia, 4–16 July 2020.

72. Zango, Z.U.; Jumbri, K.; Zaid, H.F.M.; Sambudi, N.S.; Matmin, J. Optimizations and artificial neural network validation studies for naphthalene and phenanthrene adsorption onto NH2-UiO-66(Zr) metal-organic framework. *IOP Conf. Series Earth Environ. Sci.* **2021**, *842*, 012015. [CrossRef]

73. Queiroz, R.N.; da Silva, M.G.C.; Mastelaro, V.R.; Prediger, P.; Vieira, M.G.A. Adsorption of naphthalene polycyclic aromatic hydrocarbon from wastewater by a green magnetic composite based on chitosan and graphene oxide. *Environ. Sci. Pollut. Res.* **2022**, *30*, 1–19. [CrossRef]

74. Zhu, Y.; Shi, W.; Gao, H.; Li, C.; Liang, W.; Nie, Y.; Shen, C.; Ai, S. A novel aminated lignin/geopolymer supported with Fe nanoparticles for removing Cr(VI) and naphthalene: Intermediates promoting the reduction of Cr(VI). *Sci. Total. Environ.* **2023**, *866*, 161379. [CrossRef] [PubMed]

75. Liu, B.; Cao, J.; Jiang, Y.; Yan, S.; He, H.; Shi, Y.; Xu, S.; Liang, J.; Ren, X. Adsorption of polycyclic aromatic hydrocarbons over CuZnFeAl–LDH modified by sodium dodecyl sulfate. *RSC Adv.* **2022**, *12*, 25623–25632. [CrossRef]

76. Anderson, M.J.; Whitcomb, P.J. Design of experiments. In *Kirk-Othmer Encyclopedia of Chemical Technology*; Wiley Blackwell: Hoboken, NJ, USA, 2000; pp. 1–22.

77. Muluh, N.S. Central composite design analysis and optimization of cadmium adsorption from synthetic wastewater by avocado seed activated carbon. *Int. J. Adv. Res. Dev.* **2017**, *5*, 652–661.

78. Ahmadi, S.; Fazilati, M.; Mousavi, S.M.; Nazem, H. Anti-bacterial/fungal and anti-cancer performance of green synthesized Ag nanoparticles using summer savory extract. *J. Exp. Nanosci.* **2020**, *15*, 363–380. [CrossRef]

79. Canchola, J.; Tang, S.; Hemyari, P.; Paxinos, E.; Marins, E. Correct use of percent coefficient of variation (% CV) formula for log-transformed data. *MOJ Proteom. Bioinform* **2017**, *6*, 316–317. [CrossRef]

80. Azad, F.N.; Ghaedi, M.; Dashtian, K.; Hajati, S.; Pezeshkpour, V. Ultrasonically assisted hydrothermal synthesis of activated carbon–HKUST-1-MOF hybrid for efficient simultaneous ultrasound-assisted removal of ternary organic dyes and antibacterial investigation: Taguchi optimization. *Ultrason. Sonochemistry* **2016**, *31*, 383–393. [CrossRef]

81. Azad, F.N.; Ghaedi, M.; Dashtian, K.; Jamshidi, A.; Hassani, G.; Montazerozohori, M.; Hajati, S.; Rajabi, M.; Bazrafshan, A. Preparation and characterization of an AC–Fe$_3$O$_4$–Au hybrid for the simultaneous removal of Cd^{2+}, Pb^{2+}, Cr^{3+} and Ni^{2+} ions from aqueous solution via complexation with 2-((2, 4-dichloro-benzylidene)-amino)-benzenethiol: Taguchi optimization. *RSC Adv.* **2016**, *6*, 19780–19791. [CrossRef]

82. Ahmad, A.L.; Sumathi, S.; Hameed, B.H. Adsorption of residue oil from palm oil mill effluent using powder and flake chitosan: Equilibrium and kinetic studies. *Water Res.* **2005**, *39*, 2483–2494. [CrossRef]

83. Puszkarewicz, A.; Kaleta, J. The Efficiency of the Removal of Naphthalene from Aqueous Solutions by Different Adsorbents. *Int. J. Environ. Res. Public Heal.* **2020**, *17*, 5969. [CrossRef]